



Effect of carbon nanotube pattern on the laser lift off and quantum efficiencies of near UV vertical LEDs

M.F. Tian^a, L.H. Huang^a, Y. Mei^a, R.B. Xu^a, Z.M. Zheng^a, X.L. Su^a, H. Long^{a,*}, L.Y. Ying^a, B. P. Zhang^a, K. Wang^b, T.J. Yu^b

^a School of Electronic Science and Engineering (National Model Microelectronics College), Xiamen University, Xiamen, 361005, People's Republic of China

^b School of Physics, Peking University, Beijing, 100871, People's Republic of China

ARTICLE INFO

Keywords:

Vertical LED
Ultraviolet light
Carbon nanotube
GaN
Quantum efficiency

ABSTRACT

Nowadays, ultraviolet light emitting diodes (UVLEDs) have aroused great interest in past few years for their promising application in adhesive curing, security identification and solid-state lighting etc. In gallium nitride (GaN) based LEDs, the patterned substrates and vertical devices' structure both played pivotal roles in elevating devices' performance. In this work, vertical near-UV-LEDs (405 nm) on different layers of carbon nanotube (CNT) patterns were fabricated by laser lift off (LLO), compared with the conventional lateral counterparts. The LLO threshold energy was reduced by CNTs layers. Although conventional lateral LEDs (LLEDs) exhibited highest external quantum efficiency (EQE) on 2CNTs pattern, the EQE of 3CNTs vertical LEDs (VLEDs) surpassed after LLO. The intrinsic physics mechanism, including: internal quantum efficiency (IQE), light extraction efficiency (LEE), Shockley-Read-Hall (SRH) recombination, radiative recombination and Auger effects, were analyzed by 'ABC model', Raman spectrum, X-ray Diffraction (XRD) and temperature dependence photoluminescence (TDPL).

1. Introduction

The nitride semiconductor has been extensively developed in last few decades for its outstanding optical and electrical properties, such as: adjustable band gap, excellent chemical stability and high electron mobility [1]. Besides market-dominating visible LEDs, ultraviolet light emitting diodes (UV-LED) attracted more and more attention in last five years, especially during nowadays' COVID19 period [2,3]. According to the emitting wavelength, the UV-LED is divided into three categories: UVA (320–400 nm), UVB (280–320 nm) and UVC (100–280 nm) [4]. The near-UV(NUV) and UVA-LEDs were usually applied in adhesive curing [5], security identification [6,7] and sterilization [8] etc. Although NUV-LEDs have been developed in last few years [9], the power of NUV-LEDs cannot yet satisfy people's requirement. Meanwhile, the vertical structure, flip-chip structure and patterned sapphire have been widely used in high power LED devices [10,11]. In 2019, S.J. Zhou.etc demonstrated that the crystalline quality and optical and electrical properties of 365 nm UV LEDs were improved through isoelectronic Al doping [12]. In 2020, H. Hu. etc had fabricated high crystalline quality InGaN/AlGaN multiple quantum structures on

patterned sapphire with silica array and UVLEDs with higher external quantum efficiency [13]. In 2017, S.J.Zhou.etc improved the light extraction efficiency and current spreading of FCLED by incorporating a highly reflective metallic reflector made by silver [14,15].

Our previous research has proved that CNT pattern can substantially improve the LEDs' efficiency by enhancing crystalline quality and light extraction efficiency and also reduce the threshold of laser lift off (LLO) during VLED fabrication [16,17]. In this work, lateral and vertical NUV LEDs on different layers (2,3,5,0) of CNTs patterns were fabricated. The effects of CNTs on LLO and NUV vertical LEDs' performances were analyzed. 'ABC' model, Raman Spectra, X-ray Diffraction (XRD) and temperature dependence photoluminescence (TDPL) were utilized in analyzing the SRH, radiative recombination, Auger effects and light extraction efficiency in these VLEDs [18].

2. Experiments

Carbon nanotube patterned sapphire substrate (CPSS): carbon nanotube arrays were grown on 4-inch silicon substrate by low pressure chemical vapor deposition. Then CNT arrays were then dry spun from

* Corresponding author.

E-mail address: longhao@xmu.edu.cn (H. Long).

<https://doi.org/10.1016/j.jlumin.2021.117938>

Received 18 November 2020; Received in revised form 21 January 2021; Accepted 22 January 2021

Available online 6 February 2021

0022-2313/© 2021 Elsevier B.V. All rights reserved.

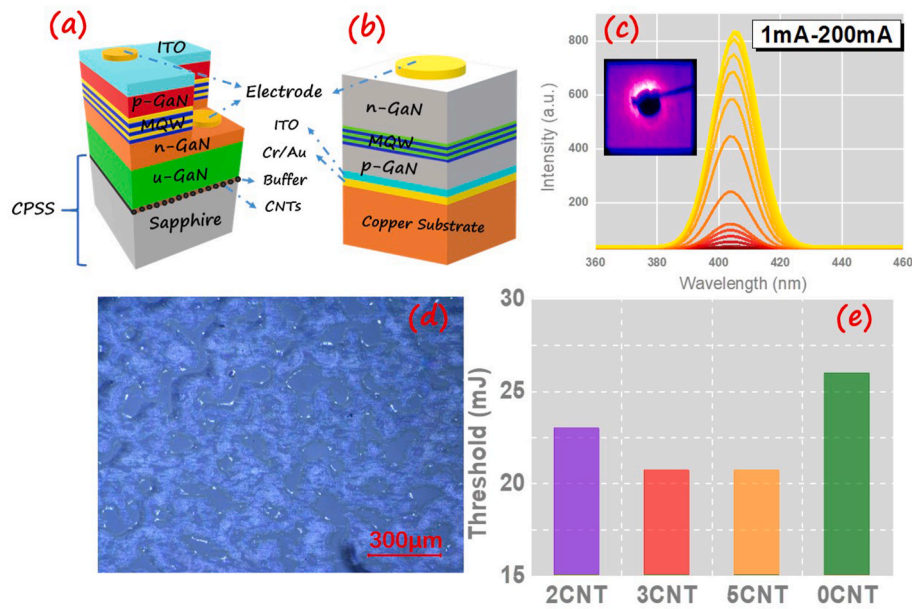


Fig. 1. (a) Structure of lateral LED and (b) vertical LED; (c) NUV EL spectra of typical LED (d) bubbles at the interface generated by LLO (e) effect of CNTs layer number to the threshold of LLO.

the CNT films, and coated onto 2inch sapphire to form CPSS. After patterned, CPSS with different layers of CNTs was dipped into ethanol and finally dried in air at room temperature [16,17]. The Nomaski and SEM image of CPSS was shown in Fig.S.1.

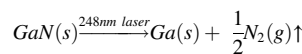
LED epitaxy and fabrication: The NUV LED wafers were grown on CPSS with 2,3,5and 0CNT patterns by metal-organic vapor phase epitaxy (MOVPE), consisting of 2 µm undoped GaN, 2 µm n-doped GaN, 10 periods of In_{0.05}Ga_{0.95}N/GaN multi quantum wells (MQWs), 200 nm p-GaN, and Indium Tin Oxide (ITO) capping transparent conductor [19]. The lateral LED (LLED) was fabricated by conventional processes, including: mesa definition, etching and electrodes' deposition. Cr/Au was used as n- and p-electrodes. As for vertical LED (VLED), after depositing Cr/Au layer on ITO surface, the 200 µm Cu was electroplated as supporting substrate, anode contact and heat sinker. Then, pulsed high power KrF (Coherent Inc., 248 nm, 25ns pulse width and 1Hz frequency) excimer laser was used to irradiate the interface between GaN buffer and sapphire to laser lift off the insulating sapphire. After peeling off the sapphire substrate, the undoped GaN layer was polished and smoothed by chemical mechanism polishing, exposing n-type GaN. Finally, cathode metal was deposited onto the polished top n-GaN surface. The sizes of LEDs were all 300x300 µm². The structure of LLED and VLED are shown in Fig. 1a and b.

Characterization: The wafer crystal was characterized by single

crystal X-Ray Diffractometer (X Pert Pro, PANalytical) with Cu Kα1 0.154 nm. Raman spectrum was recorded by Confocal Raman spectral Imaging System (WITec alpha 300RA, Witec, German) with 420 nm excitation, 0.5 nm resolution. Temperature dependent PL was measured by Andor SR500i monochromatic and CCD with Optistat-Dry cryogen system (4K-300K BL4, Oxford Instruments).

3. Results and discussion

It was worth noting that during LLO, CNTs layer number influenced the LLO threshold significantly. Particularly, CNT could reduce the laser threshold because of its high absorption coefficient, low specific heat and superior thermal conductance [16]. In LLO, laser irradiated onto the interface. High temperature (>800 °C) decomposed the GaN:



Some 'bubbles' appeared at interface during the decomposition, as shown in Fig. 1d. The sapphire could be peeled off by increasing the laser energy to threshold when 'bubble' ratio approaching 100%. In this work, we found that the thresholds of LLO were 26 mJ, 23 mJ, 20.7 mJ and 20.7 mJ when CNT layer were 0, 2, 3 and 5. The LLO threshold was reduced by CNTs layers, and saturated at 3CNTs. The lower LLO

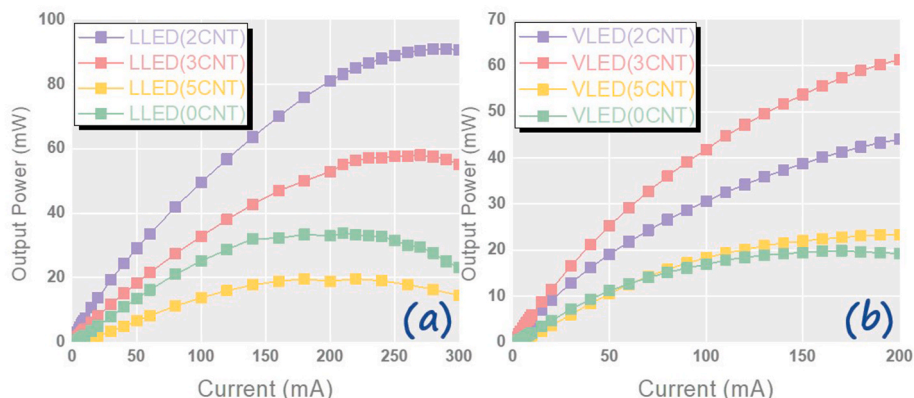


Fig. 2. (a) P-I curve of LLEDs and (b) VLEDs on various CNT layers.

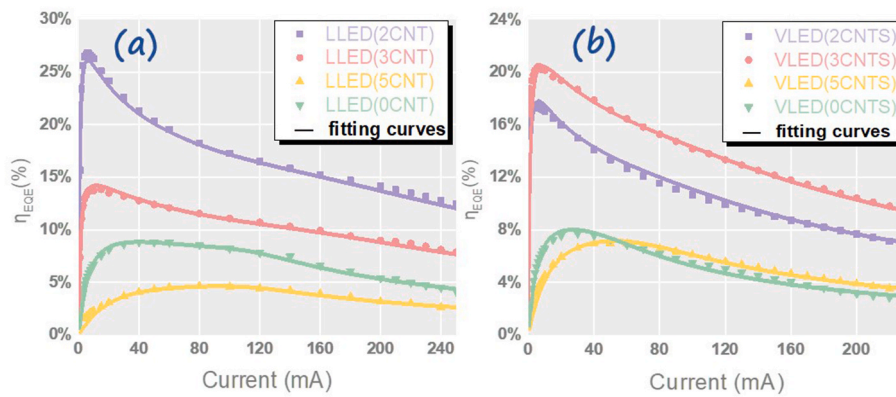


Fig. 3. (a) the EQE of LLEDs; and (b) VLEDs by ‘ABC’ fitting.

threshold brought less degradation to wafer crystal during LLO and enhanced VLEDs’ performance. In the fabrication of VLEDs, the corresponding LLO thresholds (26 mJ@0CNT-LED; 23 mJ@2CNTs-LED; 20.7mJ@3CNTs-LED and 5CNTs-LED) were applied to peel off sapphire in respective wafer to minimize the degradation by LLO.

Typical electroluminescent (EL) spectrum of 2CNTs-VLED was shown in Fig. 1c. The EL spectrum confirmed the NUV emission of 400–405 nm. The output optical power (P-I curves) of all LEDs were also characterized (Fig. 2a and b). The P-I curves show that the LLED with 2CNTs layer pattern (named as: 2CNTs-LLED) exhibited the highest light output power. The output power of 5CNTs-LLED was the lowest among these lateral devices. All the LLEDs exhibited saturate and quenching EL power by increasing injection current. Similar ranking of EL output power was also observed in 450 nm blue LEDs on different CNT layers, as reported in our previous paper [20]. Although the output power of VLEDs exhibited similar saturation behavior with LLEDs, however, other than 2CNTs-VLED, 3CNTs-VLED showed highest output power. 5CNTs-VLED and 0CNT-VLED exhibited nearly same inferior output power.

The external quantum efficiency (EQE) could be deduced by P-I curves by equation:

$$\eta_{EQE} = \frac{P/\hbar\omega}{I/q}$$

Where $P, \hbar\omega, I, q$ represented the output power, photon energy, current and electron charge, respectively [21]. The EQEs of LLEDs and VLEDs were shown in Fig. 3a and b, where the 2CNTs-LLED exhibited highest EQE. In our previous research, the CNTs pattern played as a nano mask in GaN epitaxy to reduce the dislocation density [16–20]. Whereas, 5CNTs-LLED shows the lowest EQE because that the too dense CNT induced inferior crystalline quality [20]. After LLO, the 3CNTs-VLEDs surpassed the 2CNTs-VLED, exhibiting the highest EQE. Compared with LLEDs, only EQE of 2CNTs-VLED decreases after LLO, while other devices showed higher (3CNTs-LED) or comparative (0CNTs- and 5CNTs-LEDs) EQE.

The External Quantum Efficiency (η_{EQE}) depends on Internal Quantum Efficiency (η_{IQE}) and Light Extraction Efficiency (η_{LEE}):

$$\eta_{EQE} = \eta_{IQE} \times \eta_{LEE}$$

To further analyze the effect of LLO on VLEDs, ‘ABC model’ was introduced to investigate the carriers’ recombination in quantum wells [22]. In ‘ABC model’, the carriers recombination rate R is expressed as [23,24]:

$$R = An + Bn^2 + Cn^3 + f(n)$$

where n represents the carriers’ density; An represents SRH non-radiative recombination, which is related with crystalline quality and

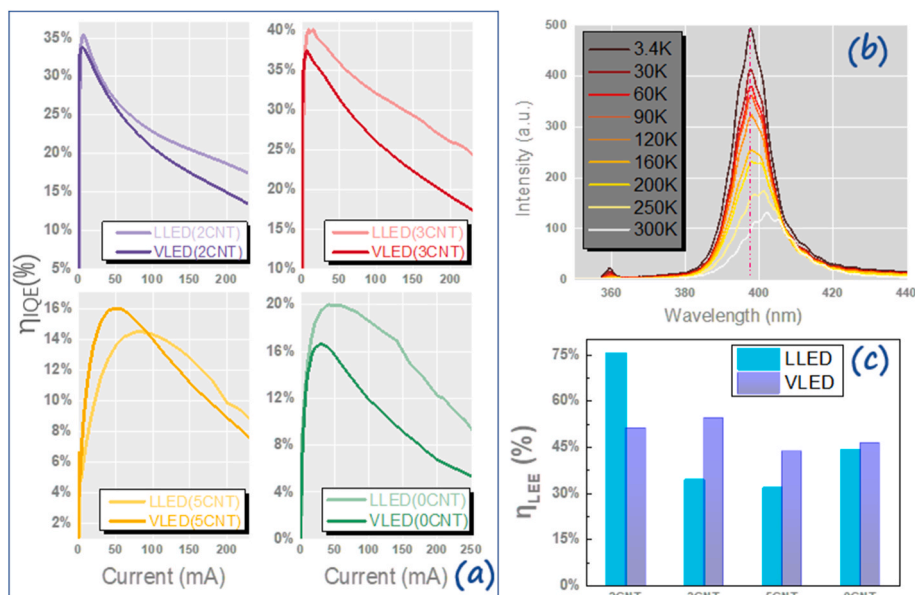


Fig. 4. (a) The IQEs of LLED and VLED; (b) The TDPL spectra of 2CNTs-LED; (c) The LEE of LLEDs and VLEDs with different CNTs layers.

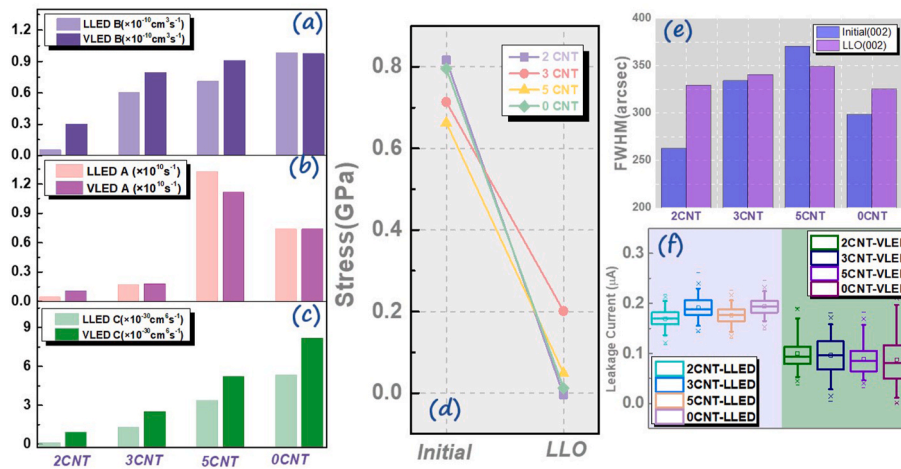


Fig. 5. (a) The radiative coefficient B of LEDs; (b) the SRH coefficient A of LEDs; (c) the Auger coefficient C of LEDs; (d) stress deduced by Raman spectra of LEDs; (e) XRD results of wafers before and after LLO; (f) reverse leakage current calculated by I-V curves.

defect density; Bn^2 corresponds to radiative recombination, which is proportional to matrix transition element of exciton dipole (see Supplementary information); the parameter C is Auger coefficient; $f(n)$ represents leakage current [25]. By introducing the ‘ABC model’, η_{IQE} and η_{LEE} of our devices could be calculated (Fig. 4a and c). In both LLEDs and VLEDs, the 3CNTs-LEDs always showed highest IQE, while the 5CNTs-LEDs always exhibited the lowest IQE. After LLO, the IQE of 2CNTs-, 3CNTs-, and 0CNT-VLEDs decreased since the degradation by high laser energy irradiation. However, the IQE of 5CNTs-VLED increases slightly, which may be ascribed with two reasons: 1. the initially poor crystalline quality of 5CNTs-LLED (proved by the lowest IQE) and thermal annealing effect induced by LLO; 2. relatively low LLO laser threshold in 5CNTs-LED (the lowest 20.7 mJ). 1.

Our IQE fitting results were also confirmed by TDPL (Fig. 4). Typical TDPL of 2CNTs-LED was shown in Fig. 4b. The IQE in TDPL was calculated by Ref. [26]:

$$\eta_{IQE} = \frac{PL \text{ Intensity } (300K)}{PL \text{ Intensity } (3.4k)}$$

The maximum IQEs of LED wafers from TDPL were 55.1% of 2CNTs-LED, 74.3% of 3CNTs-LED, 40.4% of 5CNTs-LED and 26.6% of 0CNT-LED. The 3CNTs-LED appeared the highest IQE, consistent with the ‘ABC model’.

The LEEs of the LLEDs were deduced to be 75.67% of 2CNTs-LED, 34.53% of 3CNTs-LED, 32.00% of 5CNTs-LED and 44.16% of 0CNT-LED respectively. The LEE was highest in 2CNTs-LLED and decreased by increasing CNT layers number, because that too dense CNTs also absorbed light. Two layers of CNTs were the optimized CNT layers number to balance the photon absorption and light scattering [20]. However, the absorption of CNTs was eliminated after LLO, which led to the similar LEE in VLEDs (51.34%, 54.51%, 43.64%, 46.40% in 2,3,5, 0 CNTs-VLEDs respectively). Thus, considering the enhancement of LEE after LLO and higher IQE, the EQE of 3CNTs-VLED exceeded that of 2CNTs-VLED.

To further decode IQE evolution, A, B, C coefficients were derived. In ‘ABC’ model, coefficient B gives the radiative recombination of active structure with perfect crystal. The radiative coefficient B is only affected by polarization electric fields in InGaN/GaN MQWs structure. The polarization fields could be deduced by EL peaks’ shift (see supplementary information). Therefore, the coefficients B could be acquired according to the peak wavelength-current curve (Fig.S.2). The coefficients B of LLEDs were calculated to be $5.39 \times 10^{-12} \text{cm}^3 \text{s}^{-1}$ of 2CNTs-LLED, $6.04 \times 10^{-11} \text{cm}^3 \text{s}^{-1}$ of 3CNTs-LLED, $7.10 \times 10^{-11} \text{cm}^3 \text{s}^{-1}$ of 5CNTs-LLED, and $9.85 \times 10^{-11} \text{cm}^3 \text{s}^{-1}$ of 0CNT-LLED, respectively. Higher radiative

coefficient B was ascribed with the lower QCSE effect in active MQWs. After LLO, the parameters B of VLEDs were changed to $3.01 \times 10^{-11} \text{cm}^3 \text{s}^{-1}$ of 2CNTs-VLED, $7.92 \times 10^{-11} \text{cm}^3 \text{s}^{-1}$ of 3CNTs-VLED, $9.10 \times 10^{-11} \text{cm}^3 \text{s}^{-1}$ of 5CNTs-VLED and $9.77 \times 10^{-11} \text{cm}^3 \text{s}^{-1}$ of 0CNT-VLED respectively (Fig. 5a). Compared with LLEDs, the coefficients B of 2CNTs-, 3CNTs- and 5CNTs-VLEDs increased, while the 0CNT-VLED remained nearly unchanged. The increasing of coefficient B attributed to the stress release in InGaN/GaN MQWs active layers by LLO. After LLO, the strain caused by the lattice and thermal mismatch between sapphire and GaN decreased since the elimination of sapphire substrate, leading to higher electron-hole overlap and exciton binding energy in quantum wells. Raman spectra of E_2^H peak shift also confirmed the strain decreasing in the LEDs (Fig. 5d).

The SRH recombination coefficients A of LLEDs and VLEDs were also calculated (Fig. 5b). For the LLEDs, the SRH coefficients A were $4.03 \times 10^8 \text{s}^{-1}$ of 2CNTs-LLED, $1.63 \times 10^9 \text{s}^{-1}$ of 3CNTs-LLED, $1.31 \times 10^{10} \text{s}^{-1}$ of 5CNTs-LLED and $7.34 \times 10^9 \text{s}^{-1}$ of 0CNT-LLED respectively. The coefficient A depends on the densities of non-radiative centers, including: dislocations and point defects [18]. The relatively smaller A in 2CNT- and 3CNT-LLEDs compared with 0CNT-LLED originated from the reduction of dislocation, especially edge dislocation [17]. In our previous reports, the CNTs patterns played as nano mask in GaN’s epitaxy. Edge dislocation bended around the CNT to annihilate with each other, which lead to better crystalline quality in 2CNTs- and 3CNTs- LLEDs. However, too dense CNT layers (5CNTs) were detrimental to the crystal since the excessive rough pattern, inducing the worst A in 5CNTs-LLED [20]. After LLO, the coefficients A of VLEDs were changed to $1.01 \times 10^9 \text{s}^{-1}$ of 2CNTs-VLED, $1.77 \times 10^9 \text{s}^{-1}$ of 3CNTs-VLED, $1.11 \times 10^{10} \text{s}^{-1}$ of 5CNTs-VLED and $7.45 \times 10^9 \text{s}^{-1}$ of 0CNT-VLED, respectively. The coefficients A of 2CNTs-, 3CNTs-, and 0CNTs-VLEDs increased after LLO, which was attributed to the crystalline degradation by LLO, explaining the decrease of IQE. The coefficient A in 5CNTs-VLED was lower than 5CNTs-LLED, which was in line with the IQE increase in 5CNTs-VLED. With poor crystalline quality, the 5CNTs-LED was thermal annealed by the high energy laser, improving the crystalline quality. In our previous work, the GaN/CPSS interfacial temperature was simulated by FDTD [16]. It was found that CNT with low specific heat, high thermal conductivity and absorption induced higher interfacial temperature. Therefore, high density CNT of 5 layers could increase the GaN temperature. The phenomena were also confirmed by the XRD data (Fig. 5e), in which the full-width at half maximum (FWHM) values of 2CNTs-, 3CNTs- and 0CNT-LEDs deteriorated while the one of 5CNTs-LED was improved by LLO.

Finally, the Auger coefficient C was also acquired. The coefficients C

Table 1

Comparative parameters between LLEDs and VLEDs before and after LLO.

Before - after LLO	A ($\times 10^9 \text{ s}^{-1}$)	B ($\times 10^{-12} \text{ cm}^3 \text{ s}^{-1}$)	C ($\times 10^{-32} \text{ cm}^6 \text{ s}^{-1}$)	maximum IQE	LEE	maximum EQE
2CNTs-LED	0.403–1.01	5.39–30.1	5.97–86.1	35.48%–33.77%	75.7%–51.3%	26.9%–17.3%
3CNTs-LED	1.63–1.77	60.4–79.2	125–247	40.12%–37.50%	34.5%–54.5%	13.9%–20.4%
5CNTs-LED	13.1–11.1	71–91	331–517	14.53%–15.97%	32%–43.6%	4.7%–7.0%
0CNTs-LED	7.34–7.45	98.5–97.7	529–813	20.00%–16.67%	44.2%–46.4%	8.8%–7.7%

Conclusions:

①: The defect density was reduced in 5CNTs-LED by LLO.

②: 3CNTs-LED had best IQE.

③: Light extraction efficiency was enhanced by LLO in 3CNTs-LED.

④: The EQE of 3CNTs-VLED surpassed 2CNTs-LLED after LLO.

of LLEDs with 2,3,5 and 0CNT were $5.97 \times 10^{-32} \text{ cm}^6 \text{ s}^{-1}$, $1.25 \times 10^{-30} \text{ cm}^6 \text{ s}^{-1}$, $3.31 \times 10^{-30} \text{ cm}^6 \text{ s}^{-1}$ and $5.29 \times 10^{-30} \text{ cm}^6 \text{ s}^{-1}$, compared with the $8.61 \times 10^{-31} \text{ cm}^6 \text{ s}^{-1}$, $2.47 \times 10^{-30} \text{ cm}^6 \text{ s}^{-1}$, $5.17 \times 10^{-30} \text{ cm}^6 \text{ s}^{-1}$ and $8.13 \times 10^{-30} \text{ cm}^6 \text{ s}^{-1}$ of the counterparts of VLEDs (Fig. 5c). The Auger coefficient C mainly depended on the density of carrier in active regions [27,28]. No matter LLEDs or VLEDs, coefficients C of 2CNTs- and 3CNTs-LEDs were less than 5CNTs- and 0CNT-LEDs. The lower coefficient A and C explained why IQEs of 2CNTs- and 3CNTs-LEDs were higher than 5CNTs- and 0CNT-LEDs. The coefficients C of all devices increased after LLO, which originated from the enhancement of effective injected carrier density. Fig. 5f shows that the reverse leakage currents of VLEDs were lower than the LLEDs. It means that LLO reduced the leakage current path, so the carrier densities in VLEDs' MQWs were elevated, increasing Auger effect. The improvement of leakage current in VLEDs were ascribed with two factors: a) the switching geometry from lateral to vertical LEDs: in LLEDs, currents were crowd at the edge of n-type etched down regions; while in VLEDs, currents uniformly distributed; b) the relaxation of QCSE effect in wells: due to LLO, stress in InGaN well was relaxed. The band diagram got flat, the constriction of carriers was enhanced and the leakage current was lowered.

4. Conclusion

In summary, vertical NUV-LEDs on different layers of CNT patterns were fabricated. The LLO threshold was reduced by the CNTs pattern. After LLO, the A, B, C, IQEs, LEEs and EQEs were changed, as shown in Table 1:

Several conclusions could be derived:

1. Since the poor initial crystal in 5CNTs-LLED, the crystalline quality was improved by the LLO thermal annealing effect.
2. 3CNTs-LED always had best IQE efficiency.
3. Light extraction efficiency was equalized by LLO since the elimination of CNTs.
4. The EQE performance in 3CNTs-VLED surpassed the one in 2CNTs-VLED, since the improvement of LEE and intrinsic high IQE.

We believed that our results will benefit the application of CNTs pattern into the high-power UV-VLEDs.

Author statement

M.F. Tian: Methodology, Formal analysis, Investigation, Writing - Original Draft, Visualization. L.H. Huang: Formal analysis, Investigation. Y. Mei: Methodology. R.B. Xu: Investigation. Z.M. Zheng: Investigation. X.L. Su: Investigation. H. Long: Conceptualization, Methodology, Writing - Review & Editing, Supervision, Project administration, Funding acquisition. L.Y. Ying: Methodology. B.P. Zhang: Conceptualization. K. Wang: Validation, Resources. T.J. Yu: Conceptualization, Resources.

Declaration of competing interest

The authors declare that they have no known competing financial interests or personal relationships that could have appeared to influence the work reported in this paper.

Acknowledgements

The work was supported by the Natural Science Foundation of Fujian Province of China (No. 2019J05023), the Youth Innovation Foundation of Xiamen, China(3502Z20206055) and the National Natural Science Foundation of China (61704140, 61774008).

Appendix A. Supplementary data

Supplementary data to this article can be found online at <https://doi.org/10.1016/j.jlumin.2021.117938>.

References

- [1] R.D. Dupuis, M.R. Krames, History, development, and applications of high-brightness visible light-emitting diodes, *J. Lightwave Technol.* 26 (9) (2008) 1154–1171.
- [2] J. Yan, J. Wang, P. Cong, L. Sun, N. Liu, Z. Liu, C. Zhao, J. Li, Improved performance of UV-LED by p-AlGaIn with graded composition, *Phys. Status Solidi B* (2) (2011) 461–463.
- [3] A. Fujioka, T. Misaki, T. Murayama, Y. Narukawa, T. Mukai, Improvement in output power of 280-nm deep ultraviolet light-emitting diode by using AlGaIn multi quantum wells, *APEX* 3 (4) (2010), 041001.
- [4] M. Kneissl, T.-Y. Seong, J. Han, H. Amano, The emergence and prospects of deep-ultraviolet light-emitting diode technologies, *Nat. Photon.* 13 (4) (2019) 233–244.
- [5] N. Saiki, O. Yamazaki, K. Ebe, UV/heat dual-curable adhesive tapes for fabricating stacked packages of semiconductors, *J. Appl. Polym. Sci.* 108 (2) (2008) 1178–1183.
- [6] K.R. Allakhverdiev, P. Di Lazzaro, S. Bollanti, F. Flora, L. Mezi, D. Murra, A. Torre, F. Bonfigli, R.M. Montereali, M.A. Vincenti, Extreme ultraviolet marking system for anti-counterfeiting tags with adjustable security level, in: XIX International Symposium on High-Power Laser Systems and Applications, 2013, 2012.
- [7] M.F. Barbosa, H.V. Dantas, A.S. de Pontes, W.d.S. Lyra, P.H.G.D. Diniz, M.C.U. de Araújo, E.C. da Silva, "Identification of adulteration in ground roasted coffees using UV-Vis spectroscopy and SPA-LDA, *LWT - Food Sci. Technol. (Lebensmittel-Wissenschaft -Technol.)* 63 (2) (2015) 1037–1041.
- [8] J. Zhang, L. Yuan, W. Liu, Q. Lin, Z. Wang, W. Guan, Effects of UV-C on antioxidant capacity, antioxidant enzyme activity and colour of fresh-cut red cabbage during storage, *Int. J. Food Sci. Technol.* 52 (3) (2017) 626–634.
- [9] H. Hu, S. Zhou, X. Liu, Y. Gao, C. Gui, S. Liu, Effects of GaN/AlGaIn/Sputtered AlN nucleation layers on performance of GaN-based ultraviolet light-emitting diodes, *Sci. Rep.* 7 (2017) 44627. Mar 15.
- [10] M. Liu, S. Zhou, X. Liu, Y. Gao, X. Ding, Comparative experimental and simulation studies of high-power AlGaIn-based 353 nm ultraviolet flip-chip and top-emitting LEDs, *Jpn. J. Appl. Phys.* 57 (3) (2018), 031001.
- [11] S.J. Chang, Y.C. Lin, Y.K. Su, C.S. Chang, T.C. Wen, S.C. Shei, J.C. Ke, C.W. Kuo, S. C. Chen, C.H. Liu, Nitride-based LEDs fabricated on patterned sapphire substrates, *Solid State Electron.* 47 (9) (2003) 1539–1542.
- [12] S. Zhou, H. Xu, H. Hu, C. Gui, S. Liu, "High quality GaN buffer layer by isoelectronic doping and its application to 365 nm InGaIn/AlGaIn ultraviolet light-emitting diodes, *Appl. Surf. Sci.* 471 (2019) 231–238.
- [13] H. Hu, B. Tang, H. Wan, H. Sun, S. Zhou, J. Dai, C. Chen, S. Liu, L.J. Guo, Boosted ultraviolet electroluminescence of InGaIn/AlGaIn quantum structures grown on

- high-index contrast patterned sapphire with silica array, *Nanomater. Energy* 69 (2020) 104427.
- [14] S. Zhou, X. Liu, Y. Gao, Y. Liu, M. Liu, Z. Liu, C. Gui, S. Liu, Numerical and experimental investigation of GaN-based flip-chip light-emitting diodes with highly reflective Ag/TiW and ITO/DBR Ohmic contacts, *Optic Express* 25 (22) (2017) 26615–26627. Oct 30.
- [15] S. Zhou, X. Liu, H. Yan, Z. Chen, Y. Liu, S. Liu, Highly efficient GaN-based high-power flip-chip light-emitting diodes, *Optic Express* 27 (12) (2019) A669–A692. Jun 10.
- [16] H. Long, X. Feng, Y. Wei, T. Yu, S. Fan, L. Ying, B. Zhang, Carbon nanotube assisted Lift off of GaN layers on sapphire, *Appl. Surf. Sci.* 394 (2017) 598–603.
- [17] H. Long, Y. Wei, T. Yu, Z. Wang, C. Jia, Z. Yang, G. Zhang, S. Fan, “High quality GaN epilayers grown on carbon nanotube patterned sapphire substrate by metal–organic vapor phase epitaxy, *CrystEngComm* 14 (14) (2012) 4728.
- [18] E.F. Schubert, *Light-Emitting Diodes*, second ed., Cambridge University Press, Cambridge, 2006.
- [19] X. Feng, T. Yu, Y. Wei, C. Ji, Y. Cheng, H. Zong, K. Wang, Z. Yang, X. Kang, G. Zhang, S. Fan, Grouped and multistep nanoheteroepitaxy: toward high-quality GaN on quasi-periodic nano-mask, *ACS Appl. Mater. Interfaces* 8 (28) (2016) 18208–18214. Jul 20.
- [20] M.F. Tian, X.J. Feng, H. Long, L.Y. Ying, B.P. Zhang, K. Wang, T.J. Yu, Impact of carbon nanotube pattern layers on gallium nitride-based light emitting diodes, *Semicond. Sci. Technol.* 35 (11) (2020) 115013.
- [21] E. Matioli, C. Weisbuch, Internal quantum efficiency in light-emitting diodes, in: *III-nitride Based Light Emitting Diodes and Applications*, 2017, pp. 129–161.
- [22] M.F. Schubert, S. Chhajed, J.K. Kim, E.F. Schubert, D.D. Koleske, M.H. Crawford, S. R. Lee, A.J. Fischer, G. Thaler, M.A. Banas, “Effect of dislocation density on efficiency droop in GaInN/GaN light-emitting diodes, *Appl. Phys. Lett.* 91 (23) (2007) 231114.
- [23] Q. Dai, Q. Shan, J. Wang, S. Chhajed, J. Cho, E.F. Schubert, M.H. Crawford, D. D. Koleske, M.-H. Kim, Y. Park, Carrier recombination mechanisms and efficiency droop in GaInN/GaN light-emitting diodes, *Appl. Phys. Lett.* 97 (13) (2010) 133507.
- [24] T. Wei, X. Ji, K. Wu, H. Zheng, C. Du, Y. Chen, Q. Yan, L. Zhao, Z. Zhou, J. Wang, J. Li, Efficiency improvement and droop behavior in nanospherical-lens lithographically patterned bottom and top photonic crystal InGaN/GaN light-emitting diodes, *Opt. Lett.* 39 (2) (2014) 379–382. Jan 15.
- [25] J. Cho, E.F. Schubert, J.K. Kim, Efficiency droop in light-emitting diodes: challenges and countermeasures, *Laser Photon. Rev.* 7 (3) (2013) 408–421.
- [26] B. Lu, L. Wang, Z. Hao, Y. Luo, C. Sun, Y. Han, B. Xiong, J. Wang, H. Li, K. Chen, X. Zhuo, J. Li, J. Kang, Study on optical properties and internal quantum efficiency measurement of GaN-based green LEDs, *Appl. Sci.* 9 (3) (2019) 383.
- [27] M.R. Krames, O.B. Shchekin, R. Mueller-Mach, G.O. Mueller, L. Zhou, G. Harbers, M.G. Craford, Status and future of high-power light-emitting diodes for solid-state lighting, *J. Disp. Technol.* 3 (2) (2007) 160–175.
- [28] H. Jeon, L.-W. Tu, M.R. Krames, M. Strassburg, S.Y. Karpov, Light-emitting diodes for solid-state lighting: searching room for improvements, *Light-Emitting Diodes: Materials, Devices, and Applications for Solid State Lighting XX* (2016).